# Noise-tolerant wavefront shaping in a Hadamard basis

## BAHAREH MASTIANI* AND IVO M. VELLEKOOP

*Biomedical Photonic Imaging Group, Faculty of Science and Technology, University of Twente, P.O. Box 217, 7500 AE Enschede, The Netherlands*
*\*b.mastiani@utwente.nl*

**Abstract:** Light scattering is the main limitation for optical imaging. However, light can be focused through or inside turbid media by spatially shaping the incident wavefront. Wavefront shaping is ultimately limited by the available photon budget. We developed a new 'dual reference' wavefront shaping algorithm that optimally uses the available light. Our method allows for multi-target wavefront shaping, making it suitable for transmission matrix measurements or transmitting images. We experimentally confirmed the improvement of the focus intensity compared to existing methods.

## 1. Introduction

Scattering and diffusion of light are the main limitations for optical imaging. However, wavefront shaping techniques make it possible to shape the incident wavefront so that it exactly matches the scattering properties of the medium, and form a focus through or inside it [1]. Feedback-based wavefront shaping algorithms search for the optimum incident field that maximizes some feedback signal, such as transmission into a specific output mode [2]. The task of finding the optimum wavefronts for multiple targets (output modes) is equivalent to measuring the transmission matrix (TM) of the scattering medium, up to an unknown phase factor for each row of the matrix [3]. The TM describes the input-output response of the scattering medium. Knowledge of this matrix makes it possible to focus at any arbitrary position behind the medium [4,5], to transmit images through it [3,6], or to study fundamental aspects of light scattering, such as the distribution of transmission channels [7,8].

A common procedure to find the optimum incident field with a phase-only spatial light modulator (SLM) is using the stepwise sequential algorithm (SSA) [2], as illustrated in Fig. 1(a). In this algorithm, the SLM is divided into segments, and the phase of each individual segment is varied between 0 and $2\pi$ consecutively while keeping the phase of all other segments fixed. Due to interference between light originating from the controlled segment and light originating from all other segments, the feedback signal will respond sinusoidally. By fitting these sinusoids, the TM is reconstructed [2].

The drawback of the SSA algorithm becomes apparent when many segments are used. In this case the contribution of each segment is small compared to the reference field coming from the rest of the segments, giving a low interferometric visibility of the feedback signal. This results in a low signal to noise ratio (SNR) in the measured TM elements. This low SNR is especially noticeable when the photon budget for the measurements is limited, such as in high-speed wavefront shaping [9], and in microscopy.

A method that was introduced by Popoff et al. [10] organizes the segments in a Hadamard basis. The feedback signal is measured for each Hadamard vector, allowing the TM to be reconstructed. In this method, always a large fraction of the segments is modulated, increasing the visibility of the interference signal, and consequently improving the SNR [10]. However, this technique requires part of the incident light to remain unmodulated serving as a reference field for the measurements. Since part of the light is not modulated, the contrast of the final focus is not
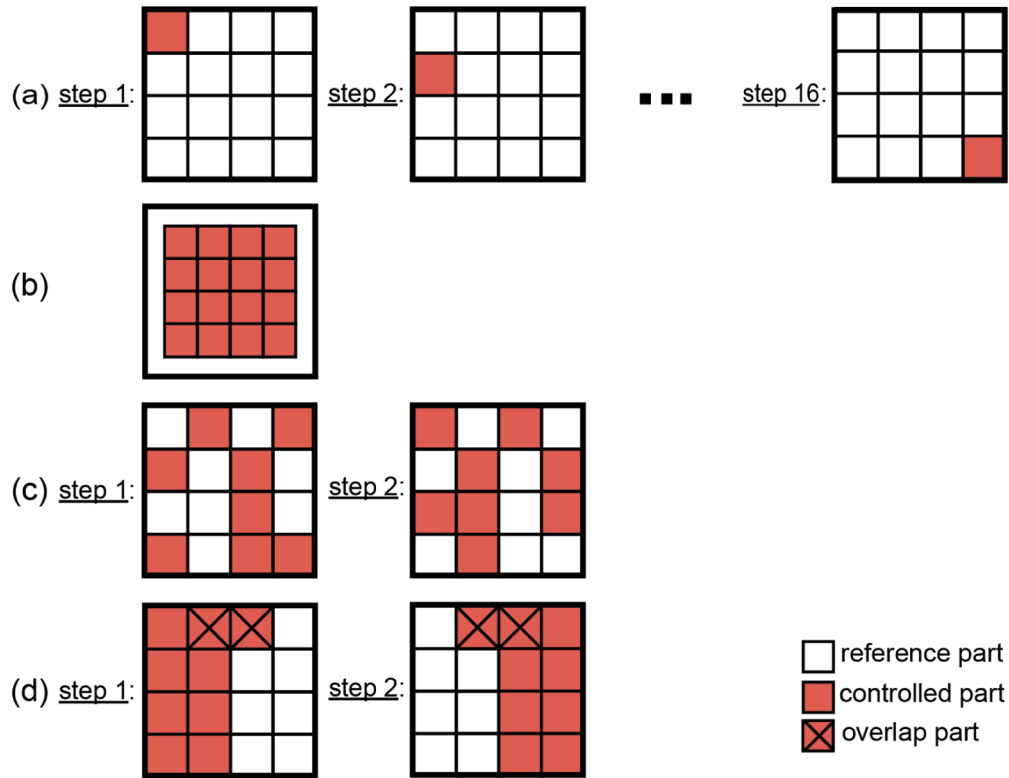
**Fig. 1.** Feedback based wavefront shaping algorithms. (a) Stepwise sequential algorithm: a single segment (in red) is controlled in every step. (b) Popoff et al. [2010] algorithm: always 65% of the SLM segments are controlled. (c) Tao et al. [2017] algorithm: in every step half of the segments are controlled. (d) Dual reference algorithm: First, a group of segments is modulated (in red), and in the second step the rest of the segments plus some overlap segments (crossed) are modulated.

optimal. This method is illustrated in Fig. 1(b), showing 65% of the SLM are always modulated (in red) and the other 35% of the segments are the reference part [10].

A different way to increase the SNR for a given photon budget is by performing a pre-optimization [11,12]. In pre-optimization schemes, one first performs an optimization with part of the SLM segments and uses that solution as a starting point for a second optimization step. With pre-optimization, the feedback signal in the second optimization step will be higher, causing the second step to be more robust to noise in most cases [11].

A special case of pre-optimization was developed by Tao et al. [12]. In the first step, half of the segments is modulated using a Hadamard-based algorithm while the other half is used as a reference. Since the number of controlled segments is equal to the number of reference segments, this approach leads to an optimally balanced interference of modulated and reference field. In the second step, the optimized half of the wavefront is displayed on the SLM. The roles of modulated and reference segment are now switched (see Fig. 1(c)), and the other half of SLM segments is optimized.

The method of Popoff et al. can be used to simultaneously find the wavefronts to focus light to multiple targets, or even to project arbitrary images through the scattering medium. In effect, this method measures multiple rows of the TM simultaneously. Unfortunately, pre-optimization approaches can not be used for this purpose. After the pre-optimization step, one has to choose

what wavefront to use as a starting point for the next step, so the procedure can only be used on one point at a time.

In this work, we present a new algorithm in a Hadamard basis, called dual reference. We chose a Hadamard basis because it is an orthogonal basis that can be perfectly made by a phase-only spatial light modulator.

The presented algorithm is a combination of the methods used by Popoff et al. [3], and Tao et al. [12]. We take advantage of the optimal balanced interference of the modulated and reference field as in Tao et al., while keeping the ability to measure all rows of the TM simultaneously, as in Popoff et al.

We will first describe our dual reference method, and explain why it outperforms other methods for a wide range of photon budgets. Afterward, we compare the experimental results of the performance of the proposed method with the existing feedback-based wavefront shaping methods for various photon budgets.

## 2. Dual reference algorithm

In our dual reference algorithm, we split the SLM segments into two groups of the same size with a small number $O$ of overlapping segments, as illustrated in Fig. 1(d). The groups have size $N_1 = (N + O)/2$, where $N_1$ is a power of two. The field in the $b$-th output mode is now given by

$$E_b = \sum_{a=1}^{N} t_{ba}E_a = \sum_{a=1}^{N_1} t_{ba}E_a + \sum_{a=N_1+1}^{N} t_{ba}E_a, \tag{1}$$

where $E_a$ is the field in the $a$-th input mode, $N$ is the total number of SLM segments, and $t_{ba}$ are the elements of the transmission matrix. In the first step, the algorithm of Popoff et al. [10] is used: a Hadamard pattern is displayed on the segments of group 1 (segments 1 to $N_1$) and the remaining segments are used as a reference. The relative phase between the two groups is changed from 0 to $2\pi$ in $P$ steps. The measured feedback signal for Hadamard vector $j \in [1, N_1]$ and phase step $k \in [1, P]$ is given by

$$I_{jk} = \left| e^{i\phi_k} \sum_{a=1}^{N_1} t_{ba}h_{ja}E_0 + E_{\text{ref},2} \right|^2. \tag{2}$$

where $h_{ja} \in \{-1, 1\}$ is the $a$-th element of the (non-normalized) $j$-th Hadamard basis vector, $E_0$ is a constant to normalize the incident field, and the reference field from group 2 is given by $E_{\text{ref},2} \equiv \sum_{a=N_1+1}^{N} t_{ba}E_a$. We omitted the subscript $b$ for brevity. Substituting $E_j \equiv \sum_{a=1}^{N_1} t_{ba}h_{ja}E_a$ gives

$$I_{jk} = \left| E_{\text{ref},2} \right|^2 + \left| E_j \right|^2 + E_{\text{ref},2}^* E_j e^{i\phi_k} + E_{\text{ref},2} E_j^* e^{-i\phi_k}. \tag{3}$$

In order to retrieve the optimized wavefront, we first perform a Fourier transform of the measured intensity

$$S_j = \frac{1}{P} \sum_{k=1}^{P} I_{jk} e^{-i\phi_k} = E_{\text{ref},2}^* E_j, \tag{4}$$

Finally, a Hadamard transform is used to convert $S_j$ to $S_{a1} = E_{\text{ref},2}^* t_{ba}E_a$. Assuming that we have an even illumination on the SLM, this gives us the transmission matrix elements $t_{ba}$ for the elements of group 1 (elements 1 to $N_1$, denoted as $a1$), up to an unknown overall factor $E_{\text{ref},2}^*$.

Our modification to Popoff's algorithm is to add a second step, where the segments of group 2 (elements $N - N_1 + 1$ to $N$, denoted as $a2$) are modulated, and the rest of the segments are now used as a reference. These two steps are shown in Fig. 1(d) with the modulated SLM segments in red and the overlap segments as crossed segments. Since the number of controlled segments is

close to the number of reference segments for all measurements, the modulated and reference fields have almost equal average contribution to the field at point $b$. This 50/50 choice for the reference and modulated part guarantees the maximal interferometric visibility and minimal sensitivity to noise for a given photon count.

After completing the two steps, we have the corrected wavefronts for group 1, corresponding to $S_{a1}$, and for group 2, $S_{a2}$. To find the final optimal wavefront, these two partial corrections need to be combined. However, since the two groups used different reference fields in the measurements, the two partial wavefronts will have a different phase offset. Since the overlap segments are present in both groups, these segments can be used for determining the relative phase between the two corrections. Denoting the overlap segments as $a = 1..O$, we compute the relative phase from the dot product of the two measurements for these overlapping segments

$$\arg\left(E_{\text{ref},2}\right) - \arg\left(E_{\text{ref},1}\right) = \arg \sum_{a=1}^{O} S_{a1} S_{a2}^* \tag{5}$$

and the relative amplitude follows from

$$\frac{\left|E_{\text{ref},2}\right|^2}{\left|E_{\text{ref},1}\right|^2} = \frac{\sum_{a=1}^{O} |S_{a1}|^2}{\sum_{a=1}^{O} |S_{a2}|^2} \tag{6}$$

After compensating the relative phase and amplitude of the two partial wavefronts, these two wavefronts can be combined into a single wavefront.
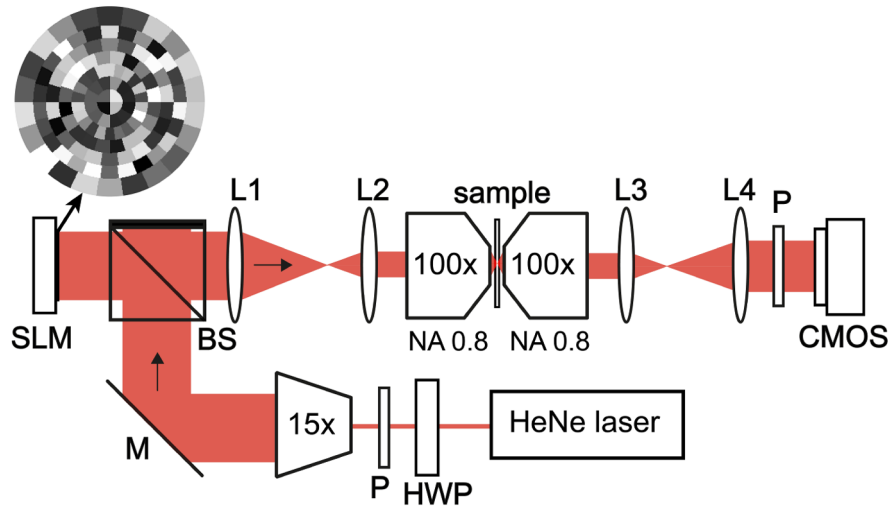
## 3. Experiment

Now, we will experimentally compare the performance of the dual reference algorithm to the original SSA algorithm and to the methods of Popoff and Tao. Since Tao's method can only measure one row of the TM at the time (hence only focus on one target), the comparison with that method is not completely fair. For completeness, we do include the method in the comparison, using only a single target in the measurements.

The experimental setup is illustrated in Fig. 2. In this setup, light from a HeNe laser (Thorlabs, 2mW, $\lambda = 632.8$ nm) is expanded and modulated by a phase-only spatial light modulator (Hamamatsu X13138-07). A 4f system images the SLM onto the back focal plane of a microscope objective (A-Plan 100x/0.8, Zeiss), which focuses the light onto the sample. After transmitting through the sample, the light is collected by an identical objective lens and recorded by a CMOS camera (Basler acA640-750um). The camera records the intensity distribution at the back focal plane of the second objective. A set of 100 independent targets on the camera is used as the feedback for the wavefront shaping algorithms.

The sample is an $11\pm3$ μm thick layer of zinc-oxide (Sigma Aldrich, average grain size 200 nm) on a coverslip with a thickness of 170 μm. The transport mean free path of similar zinc oxide samples was measured to be around 0.6 μm at a wavelength of $\lambda = 632.8$ nm [13]. Consequently, the sample is optically thick so that there is no transmitted ballistic light. The sample is mounted on a translation stage (Zaber T-LSM050A) to scan the sample laterally for ensemble averaging.

The beam illuminating the SLM has a Gaussian intensity profile. It is well known that such a non-uniform illumination causes a sub-optimal enhancement [14]. To overcome this effect, we choose a circular geometry instead of the common rectangular one, as is shown in Fig. 2(inset). The sizes of the rings are adjusted such that each segment, on average, contributes equally to the target signal. This way, the illumination effectively is uniform, and the enhancement is maximized.

To control the photon budget used in the experiments, we used various neutral density filters with different transmission ratios in front of the camera. The power of detected light was

**Fig. 2.** Schematic of the experimental setup. HWP, half-wave plate; M, mirror; BS, 50% non-polarizing beam splitter; P, polarizer; CMOS, complementary metal oxide semiconductor camera; L1, L2, L3 and L4, lenses with focal length of respectively 200 mm, 75 mm, 75 mm and 150 mm. The inset shows a random wavefront displayed on the modulating segments of the SLM

measured by a calibrated power meter (S121C, Thorlabs). The measured power is converted to the photon count collected by the camera. We kept increasing the total photon budget as long as the camera did not reach saturation during the measurement.

In the wavefront shaping experiments, we measured the enhancement of the focus, defined as the ratio of the optimized intensity at the focus location to the reference intensity which is the averaged intensity over 100 positions for the sample [1].

In our experiments, measuring the corrected wavefront for one target took 50 seconds. For more than one target, this time interval does not change for all the algorithms except for Tao's method, which is linearly increased with the number of targets.
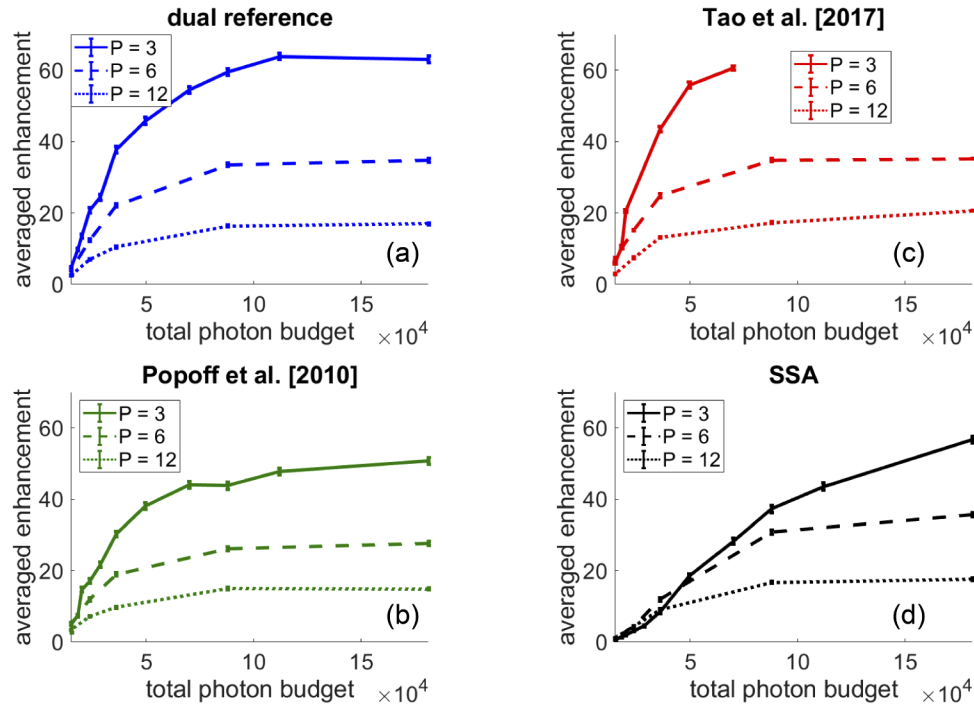
## 4. Optimal number of phase steps

All four algorithms require the choice of two parameters: the number of SLM segments ($N$) and the number of phase steps per segment ($P$). Together, these parameters determine the total number of measurements $NP$. It is well known that in absence of noise the expected enhancement scales linearly with $N$ [15], so $N$ should be chosen as high as possible, resulting in a minimal number of phase steps $P = 3$. In presence of noise, however, the relation is more complicated, and different types of noise (such as read-out noise, shot noise and laser excess noise) affect the results in different ways [11]. When the number of measurements $NP$ is fixed, a higher value of $P$ will give a more accurate measurement of each transmission matrix element, at the expense of decreasing $N$.

To find the optimum value for $P$ for the different algorithms, we measured the enhancement for different combinations of $P$ and $N$. To enable a fair comparison, we choose the number of SLM segments in a way that all algorithms have the same number of measurements. For the lowest phase steps number ($P = 3$), we set 128 segments for Tao's method [12] and SSA. For Popoff's method [3] the SLM is divided into 197 segments, out of which 128 segments are modulated, and the remaining 69 segments (35%) serves as the reference. For our dual reference algorithm, we had 123 modulated segments with 5 segments mutual in two 64-segment groups. As a result,

the number of measurements for all the algorithms is the same, and equal to 384. We kept this number fixed by reducing the number of segments by two or four when $P$ is respectively 6 and 12.

For the dual reference algorithm, SSA, and Popoff's method, we executed the algorithm once to simultaneously find the optimized wavefronts for focusing at multiple different points. We then displayed the wavefronts on the SLM individually to measure the enhancement of each focus. However, for Tao's method the optimization had to be done point by point.

Figure 3 shows the averaged enhancement over 100 targets and 3 trials versus total photon budget when $P$ is 3 (solid curve), 6 (dash curve), and 12 (dot curve). For the dual reference method Fig. 3(a), Popoff's method Fig. 3(b), and Tao's method Fig. 3(c), the highest enhancement for every photon budget is obtained for $P = 3$. However, Fig. 3(d) shows that for a photon budget lower than $5 \cdot 10^4$, SSA shows a slightly better performance for larger values of $P$.



**Fig. 3.** The measured averaged enhancement versus the total photon budget when the number of phase steps is 3 (solid), 6 (dash), and 12 (dot), (a) for dual reference algorithm, (b) Popoff et al. [10], (c) Tao et al. [12], and (d) SSA. Bars represent the standard error of the measurement set.

For Tao's method, during step 2, the corrected wavefront from step 1 is displayed on the SLM, causing the camera to be overexposed for higher photon budgets. For this reason, there are fewer reported measurements for Tao's method than for the other methods.

The results from Fig. 3 show that a lower $P$ with higher $N$ is better than performing accurate measurements for fewer segments. Therefore, we set $P = 3$ for all algorithms and compare the performance of the dual reference algorithm with the other algorithms.

## 5. Results and discussion

After choosing the optimum number of phase steps, we measured the enhancement for different methods. Figure 4 illustrates the measured enhancement averaged over 100 targets (optimized in a single run of the algorithm) and repeating the experiment 3 times for dual reference, SSA

and Popoff's method. The measured enhancement for Tao's method is averaged over 10 targets (optimized in 10 separate runs of the algorithm) and 3 trials. The error bars are statistical error bars obtained by averaging over the targets and repeating experiments 3 times. Besides the plotted error bars, there is an additional variation of approximately ±15% between the different experiments that may be caused by experimental factors such as sample drift and alignment. For all algorithms, the overall enhancement increases as the total photon budget increases since the signal to noise ratio increases.
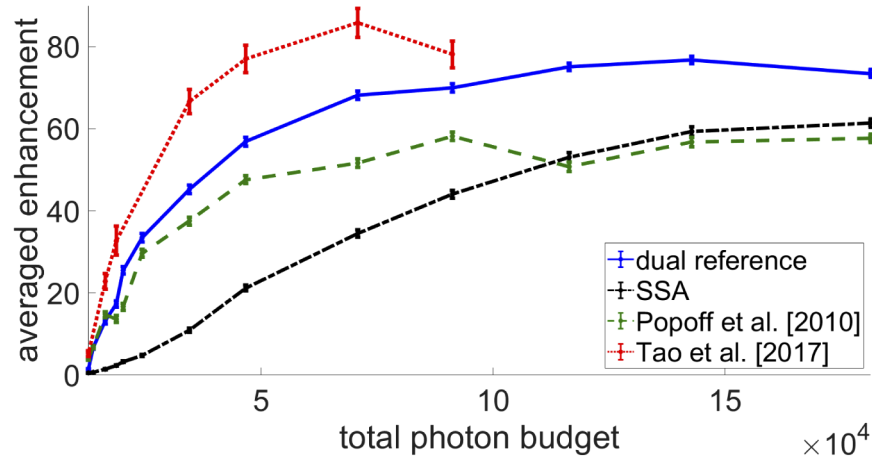


**Fig. 4.** The measured averaged enhancement versus the total photon budget for dual reference algorithm (blue solid curve), SSA (black dash-dot curve), Popoff et al. [10] (green dash curve), and Tao et al. [12] (red dot curve). Bars represent the standard error of the measurement set.

The measured enhancement for Tao's method, shown in the red dot curve in Fig. 4, is higher than the other algorithms due to the pre-optimization step. However, the comparison is not completely fair. In Tao's method, the wavefront used as reference in the second step of the algorithm is different for every target, which makes it impossible to do simultaneous multi-target optimization. Therefore, when optimizing $M$ targets, the required measurement time and photon budget will be $M$ times larger than with the other methods.

The measured enhancement for the dual reference algorithm, shown as the blue solid curve in Fig. 4, confirms that using this method gives us higher enhancement for multi-target optimization compared to SSA (black dash-dot curve) and Popoff's method (green dash curve). This improvement comes from the optimum interferometric visibility during the measurements, resulting in an optimal SNR and consequently higher enhancement.

For a high photon budget, we theoretically expect to have an enhancement of $N\pi/4$ for SSA, dual reference, and Tao's methods, and $0.65N\pi/4$ for Popoff's method. In our experiments, the measured enhancement for the highest photon budget ($1.8 \cdot 10^5$ photons) is 25 % lower than the expected enhancement from the theory. This difference can be explained by practical imperfections, such as the static (non-modulated) field caused by the reflection of the SLM front surface. In our case, this static field has an amplitude of 10 % of the input field amplitude.

## 6. Conclusion

With the advance of high-speed SLMs, the photon budget will ultimately be the limiting factor for wavefront shaping. We have presented a new feedback-based wavefront shaping algorithm to optimally use the available light.

We demonstrated that for a fixed number of measurements the best performance of all algorithms is reached by minimizing the number of phase steps.

Our algorithm achieves the maximal interferometric visibility during the measurements, resulting in an optimal SNR. Moreover, there is no need to reserve segments for the reference beam. We have experimentally demonstrated that this method enables us to perform simultaneous multi-target optimization with a higher enhancement than the popular methods used by Popoff et al. [2010] and Tao et al. [2017] (for multi-target) for a wide range of photon budgets.

We envision that the presented method could be beneficial to the experiments having the transmission matrix measurement involved, especially when the photon budget is limited.

**Disclosures.** The authors declare no conflicts of interest.

**Data availability.** Data underlying the results presented in this paper are not publicly available at this time but may be obtained from the authors upon reasonable request.

## References

1. J. Kubby, S. Gigan, and M. Cui, *Wavefront shaping for biomedical imaging* (Cambridge University, 2019).
2. I. M. Vellekoop, "Feedback-based wavefront shaping," Opt. Express **23**(9), 12189–12206 (2015).
3. S. Popoff, G. Lerosey, M. Fink, A. C. Boccara, and S. Gigan, "Image transmission through an opaque material," Nat. Commun. **1**(1), 81–85 (2010).
4. H. Yu, T. R. Hillman, W. Choi, J. O. Lee, M. S. Feld, R. R. Dasari, and Y. Park, "Measuring large optical transmission matrices of disordered media," Phys. Rev. Lett. **111**(15), 153902 (2013).
5. M. Kim, W. Choi, Y. Choi, C. Yoon, and W. Choi, "Transmission matrix of a scattering medium and its applications in biophotonics," Opt. Express **23**(10), 12648–12668 (2015).
6. A. P. Mosk, A. Lagendijk, G. Lerosey, and M. Fink, "Controlling waves in space and time for imaging and focusing in complex media," Nat. Photonics **6**(5), 283–292 (2012).
7. H. Yılmaz, C. W. Hsu, A. Yamilov, and H. Cao, "Transverse localization of transmission eigenchannels," Nat. Photonics **13**(5), 352–358 (2019).
8. S. Rotter and S. Gigan, "Light fields in complex media: Mesoscopic scattering meets wave control," Rev. Mod. Phys. **89**(1), 015005 (2017).
9. D. Feldkhun, O. Tzang, K. H. Wagner, and R. Piestun, "Focusing and scanning through scattering media in microseconds," Optica **6**(1), 72–75 (2019).
10. S. Popoff, G. Lerosey, R. Carminati, M. Fink, A. Boccara, and S. Gigan, "Measuring the transmission matrix in optics: an approach to the study and control of light propagation in disordered media," Phys. Rev. Lett. **104**(10), 100601 (2010).
11. H. Yılmaz, W. L. Vos, and A. P. Mosk, "Optimal control of light propagation through multiple-scattering media in the presence of noise," Biomed. Opt. Express **4**(9), 1759–1768 (2013).
12. X. Tao, T. Lam, B. Zhu, Q. Li, M. R. Reinig, and J. Kubby, "Three-dimensional focusing through scattering media using conjugate adaptive optics with remote focusing (CAORF)," Opt. Express **25**(9), 10368–10383 (2017).
13. E. G. van Putten, "Disorder-enhanced imaging with spatially controlled light," Ph.D. thesis, University of Twente (2011).
14. D. Akbulut, T. J. Huisman, E. G. van Putten, W. L. Vos, and A. P. Mosk, "Focusing light through random photonic media by binary amplitude modulation," Opt. Express **19**(5), 4017–4029 (2011).
15. I. M. Vellekoop and A. P. Mosk, "Focusing coherent light through opaque strongly scattering media," Opt. Lett. **32**(16), 2309–2311 (2007).